Volume 8
Number 12
28 March 2020
Pages 3925–4280

Journal of Materials Chemistry C

Materials for optical, magnetic and electronic devices

rsc.li/materials-c

ISSN 2050-7526

ROYAL SOCIETY OF CHEMISTRY

PAPER

Bingfu Lei *et al.*

Glass-ceramics with thermally stable blue-red emission for high-power horticultural LED applications

Journal of Materials Chemistry C

ROYAL SOCIETY OF CHEMISTRY

PAPER

View Article Online
View Journal | View Issue

Cite this: J. Mater. Chem. C, 2020, 8, 3996

Glass-ceramics with thermally stable blue-red emission for high-power horticultural LED applications†

Weibin Chen,[a] Xuejie Zhang,[ab] Jianxian Zhou,[a] Haoran Zhang,[a] Jianle Zhuang,[ab] Zhiguo Xia,[c] Yingliang Liu,[ab] Maxim S. Molokeev,[de] Gening Xie[a] and Bingfu Lei *[ab]

Received 6th January 2020,
Accepted 7th February 2020

DOI: 10.1039/d0tc00061b

rsc.li/materials-c

As one of the key elements of indoor agriculture, horticultural light sources are developing rapidly towards requiring high energy density, high output power and high stability, which poses a challenge for traditional phosphor conversion devices. To address this, an all-inorganic blue-red dual-emitting light convertor consisting of $Ba_{1.3}Sr_{1.7}MgSi_2O_8:Eu^{2+},Mn^{2+}$ (BSMS) phosphor-in-glass (PiG) plates was prepared to improve the duration lifetime of converted high-power light-emitting diodes (LEDs) and meet the light quality requirements of photosynthesis for indoor agriculture. The obtained samples show an external quantum efficiency of 45.3%, outstanding thermal stability and a specific emission spectrum that highly matches the absorption of chlorophyll and β-carotene. Moreover, a proof-of-concept BSMS-PiG horticultural lamp for application in an indoor plant factory was successfully fabricated based on a ~370 nm emitting LED chip. The blue-red ratio of its spectrum could be regulated by controlling the thickness of BSMS-PiG and the concentrations of Mn^{2+} ions within BSMS-PiG. The BSMS-PiG horticultural LEDs were applied to the indoor cultivation of Romaine lettuce. The results indicated that the biomass of Romaine lettuce was 58.21% greater than that of control lettuce samples cultivated under commercial plant lamps. In particular, the content values of total chlorophyll, β-carotene and soluble protein were improved. The BSMS-PiG horticultural LED is a potential candidate to act as a high-power horticultural light source.

1 Introduction

Farmland soil suffers varying degrees of contamination, which has caused a serious threat to food safety, the ecological environment and sustainable agricultural development.[1,2] To supply enough food for a rapidly expanding population, agriculture has to be intensified to solve the contradiction between population, resources and the environment. Consequently, indoor artificial plant factories, as a new model of agriculture, have come into being and have achieved greater development.[3]

Light energy is at the core of the plant factory and one of the essential conditions for plant growth and ontogeny. It affects plant metabolism and development of vegetation processes.[4] The energy distributions in the blue (400–500 nm), red (600–690 nm), and far red (720–740 nm) regions play a key role in phototropic processes, photosynthesis, and plant photomorphogenesis, respectively.[5] For indoor agriculture, light-emitting diodes (LEDs) are a very promising technology that provide a variety of possibilities for horticultural lighting.[6] Compared with traditional light sources for plant growth such as halogen lamps or high pressure sodium lamps, LEDs have high luminous efficiency, low power consumption, long life and other technical advantages.[7] LEDs have emission peaks ranging from UV-C (~250 nm) to infrared (~1000 nm), and the specific spectrum composition can be controlled with light convertors.[8] For this reason, LED lighting technology provides highly controllable lighting conditions to increase productivity and control over horticultural production. In addition, the intensity of light is a significant factor affecting plant growth.[9]

[a] Guangdong Provincial Engineering Technology Research Center for Optical Agriculture, College of Materials and Energy, South China Agricultural University, Guangzhou 510642, P. R. China. E-mail: tleibf@scau.edu.cn
[b] Guangdong Laboratory of Lingnan Modern Agriculture, and Key Laboratory for Modern Agriculture Materials of Ministry of Education, Guangzhou 510642, P. R. China
[c] The State Key Laboratory of Luminescent Materials and Devices, and Guangdong Provincial Key Laboratory of Fiber Laser Materials and Applied Techniques, School of Materials Science and Engineering, South China University of Technology, Guangzhou 510641, P. R. China
[d] Laboratory of Crystal Physics, Kirensky Institute of Physics, Federal Research Center KSC SB RAS, Krasnoyarsk 660036, Russia
[e] Siberian Federal University, Krasnoyarsk 660041, Russia

† Electronic supplementary information (ESI) available. See DOI: 10.1039/d0tc00061b

High-intensity illumination is beneficial for secondary metabolic processes of plants, such as self-repair and active oxygen quenching.[10] This has forced horticultural light source development towards high energy density, high output power and high stability, which poses a challenge for phosphor conversion devices.[11,12]

To solve this problem, all-inorganic luminescent glass ceramics have been proposed through the continuous efforts of researchers. They solve the serious aging problem of traditional fluorescent powders and silicone composite materials with their excellent physical and chemical stability.[13,14] For instance, Chen *et al.*[15] enhanced the luminescence of $Y_3Al_5O_{12}:Mn^{4+}$ by impurity doping and fabricated a colour convertor through a phosphor-in-glass (PiG) approach. Wang *et al.*[16] reported a bright red-emitting phosphor $BaMgAl_{10}O_{17}:Mn^{4+},Mg^{2+}$ and embedded the phosphor into an oxide glass matrix to replace phosphor-in-organic silicone (PiS). Deng *et al.*[17] prepared an ultrastable red-emitting glass ceramic using a $3.5MgO{\cdot}0.5MgF_2{\cdot}GeO_2:Mn^{4+}$ PiG matrix for superior high-power artificial plant growth LEDs. Furthermore, Li *et al.*[18] reported a spliced highly efficient dual-broadband emitting light convertor, in which $BaMgAl_{10}O_{17}:Eu^{2+}$ and $CaAlSiN_3:Eu^{2+}$ provided blue and red emission, respectively. However, the above-reported light convertors have many shortcomings. Either the emission peaks in the blue region are too narrow to fully match the absorption spectrum of plant photosynthesis,[19,20] or the preparation processes are complex, and excitation light leaks through the patchwork seams.[21] Narrow-band blue-light emission cannot fully meet the physiological needs of plants[22] and the UV light coming from the splicing gap of PiG is wasted. To foster the strengths and circumvent the weaknesses, the light converting material should display dual-broadband emission and no light leakage, as well as superior stability.

Hence, the choice of the fluorescent component is especially important for all-inorganic glass ceramics which are to be used on high-power plant lamps. The phosphor $(Ba,Sr)_3MgSi_2O_8$ co-doped with Eu^{2+} and Mn^{2+} has been used for color correction in agricultural lamps because of the intense blue- and red-emission bands.[23–25] Structurally optimized $Ba_{1.3}Sr_{1.7}MgSi_2O_8:Eu^{2+},Mn^{2+}$ (BSMS) possesses emission bands at 430 nm and 660 nm suitable for plant photosynthesis. Mao *et al.*[26] determined its structure and determined the optimal doping amount of Eu^{2+} ions as 6%. It is a very promising material for the fluorescent component of luminescent glass ceramics in monolithic light converting materials. For high-power LEDs, phosphor devices must have excellent thermal stability to withstand the heat emitted by the LED chips. At present, however, the BSMS phosphor convertor does not meet the requirements for use with high-power LEDs.

Inspired by the previous progress, in this work, a high-power light converting device with blue and red dual-broadband emission is reported. It was prepared by the PiG approach, improving the service life and solving the problem of light leakage, and is composed of a glass matrix with embedded BSMS phosphors. The microstructure, luminescence properties and thermal stability of BSMS-PiG were meticulously investigated. Our results are consistent with the analysis of Deng *et al.* and Li *et al.*, in that the photoluminescence (PL) of the BSMS phosphor can be well maintained in PiG and the thermal stability of BSMS-PiG is better than that of phosphor. Furthermore, in order to adapt to the growth needs of various plants, the red-blue ratio of BSMS-PiG-converted ~370 nm LED chips was regulated by controlling the thickness of BSMS-PiG and the concentration of Mn^{2+} ions in the BSMS-PiG. Meanwhile, 7 wt% BSMS-PiG plates were applied in high-power horticultural LEDs to improve the growth of Romaine lettuces.

2 Experimental

2.1 Phosphor preparation

Phosphor samples with an optimized nominal composition of $Ba_{1.3}Sr_{1.7}MgSi_2O_8$: 6% Eu^{2+},*x*% Mn^{2+} with $x = 1, 2, 3, 4, 5$ and 6 were prepared by a conventional solid reaction method. The reagents were $BaCO_3$ (99.9%, Aladdin), $SrCO_3$ (99.9%, Aladdin), MgO (99.9%, Aladdin), SiO_2 (99.9%, Aladdin), Eu_2O_3 (99.9%, Aladdin) and $MnCO_3$ (99.9%, Aladdin). The six raw materials were mixed entirely with fluxing agent (5% of NH_4Cl) and a suitable amount of ethanol in an agate mortar and then dried at 80 °C for 1 h. Then each mixture was sintered in a corundum crucible at 1250 °C for 8 h under a reducing gas atmosphere (5% H_2–95% N_2). Finally, the naturally cooled samples were ground to a fine powder to provide the fluorescent component of PiG.

2.2 Light convertor synthesis

Precursor glass with the composition (mol%) of $38SiO_2$–$10B_2O_3$–$12ZnO$–$15Na_2O$–$5K_2O$–$5Al_2O_3$–$15CaO$ was prepared. The mixed raw materials were heated at 1350 °C for 1 h in a corundum crucible. After cooling, the glass was milled into a glass frit. The relative ratio of the BSMS phosphor to glass matrix was fixed in the range of 1–7 wt%. A series of BSMS-PiG samples was prepared by mixing phosphor particles and glass frit in an agate mortar, and then the powder mixtures were compressed into sheets under 30 MPa pressure and sintered at 585 °C for 1 h under a reducing gas atmosphere (5% H_2–95% N_2). Similar phosphor-in-silicone (PiS) samples were synthesized by dispersing the BSMS phosphor in organic silicone (purchased from DC184 silicone of Dow Corning).

2.3 Plant cultivation

Indoor Romaine lettuce cultivation experiments were conducted by hydroponics under different photosources including BSMS-PiG-converted ~370 nm LEDs chips, and reference commercial plant lamps (Model JL-2835-60W, Dongguan Longfar Optoelectronics Technology Co., Ltd). All Romaine lettuce samples at seedling growth stage were initially cultivated for 14 days under identical illumination conditions and in the same environment, and then they were transplanted indoors to grow for 7 days with the above-mentioned different light treatments (intensity 80–100 μmol m^{-2} s^{-1} photosynthetic photon flux density). The environmental temperature was 22 ± 3 °C, the humidity was ~60–65%, and the carbon dioxide concentration was 340 ± 20 ppm. Shoot weights (fresh and dry) were measured

and the data from 4 random plants were averaged, while additional indicators were obtained from 4 samples. All indicators were gauged according to previously disclosed methods.[27,28]

2.4 Characterization

Powder X-ray diffraction (XRD) was performed on Bruker Ultima-IV X-ray diffractometer with Cu Kα (λ = 1.5405 Å) radiation at 40 kV and 40 mA. The morphologies and elemental compositions were measured by scanning electron microscopy (SEM), using a microscope equipped with an energy dispersive spectroscopy (EDS) system (Hitachi SU8220, Japan). Confocal laser scanning microscopy (CLSM) images were collected with a confocal laser scanning microscope (DM6000 B, LEICA), equipped with a 405 nm laser as an excitation source. The photoluminescence excitation (PLE) and photoluminescence emission (PL) spectra in the temperature range 298–478 K were measured using a F-7000 fluorescence spectrometer (Hitachi, Ltd, Japan) equipped with a 150 W xenon lamp as an excitation source. The quantum efficiencies and absorption efficiencies were measured using a FLS1000 spectrometer (Edinburgh Instruments, Britain). The heat transfer phenomena of the BSMS-PiG-converted LED chips and BSMS-PiS-converted LED chips with 1 A current were studied using a FLIR E40 infrared camera (FLIR System, Inc., United States). The irradiances of the high-power horticultural LEDs were measured using a TA8123 digital light meter (Suzhou TASI Electronics Co., Ltd, China).

3 Results and discussion

In order to inspect the possible reaction between the phosphor and glass, SEM, EDS, and EDS mapping were carried out. In Fig. 1a, it is clearly seen that the BSMS phosphor particles are embedded in the glass matrix. The elements including Na, Zn, Sr, Ba and Mg are distributed quite homogeneously in the EDS mapping images of BSMS-PiG. The Na- and Zn-rich regions represent the glass matrix, while the Sr-, Ba- and Mg-rich portions indicate the phosphor particles. These SEM and EDS mapping characterizations all indicate that the BSMS phosphor particles are integrated as the powder in the glass matrix.

To clearly observe the distribution of the BSMS phosphor powder inside the glass matrix, CLSM was employed using a laser wavelength of 405 nm. In Fig. 1b, a pink emission can be observed in the PiG under 365 nm UV light, determining initially that the BSMS phosphor had been integrated into the glass matrix. The horizontal fluorescence distribution of the BSMS phosphor particles inside the PiG is clearly shown in Fig. 1c. The pink light-spots indicate phosphor particles, while the rest of the area represents glass matrix. Based on the above results, a conclusion can be drawn that the BSMS phosphor particles are uniformly dispersed in the glass matrix. Moreover, a uniform spatial distribution of 7 wt% BSMS phosphor in PiG is also shown in Fig. 1d and e to illustrate the homogeneous distribution of phosphor particles in the PiG sample.

The PLE and PL spectra of BSMS-PiG and the corresponding BSMS phosphor powder are shown in Fig. 2a. The excitation spectra exhibit band emission ranging from UV to near-UV with a main peak at around 355 nm (due to the 4f–5d transition of Eu^{2+}). The PL spectra of BSMS-PiG and the BSMS phosphor display dual-emission, consisting of a 430 nm blue emission band arising from the electric-dipole allowed $4f^65d^1 \rightarrow 4f^7$ transition of Eu^{2+} ions and a 660 nm red emission band resulting from the $^4T(^4G) \rightarrow {}^6A_1(^6S)$ transition of the $3d^5$ energy level of Mn^{2+} ions.[29] The luminescence properties of BSMS-PiG and the BSMS phosphor are similar to one another in terms of the location of both the excitation and emission bands.

All of the BSMS-PiG and BSMS samples have similar decay curves because of the representative $4f^65d^1 \rightarrow 4f^7$ electric-dipole transition of Eu^{2+}. As demonstrated in Fig. 2b, these decay curves could be well fitted to a typical single exponential function, and the Eu^{2+} lifetime of 7 wt% BSMS-PiG was determined to be about 218.09 ns, which is close to the 212.69 ns lifetime of Eu^{2+} in the BSMS phosphor. These results prove that the fluorescence lifetime is not affected by the glass matrix.

Fig. 2c shows that the PL intensity of BSMS-PiG can be improved by increasing the phosphor doping concentration, and the maximum value appears at 7.0 wt%. The internal quantum efficiency (IQE), external quantum efficiency (EQE) and absorption efficiency (AE) of BSMS-PiG and the BSMS phosphor were

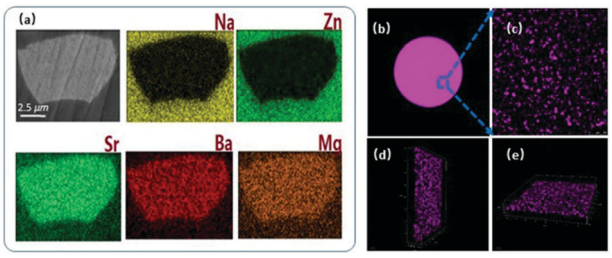

Fig. 1 (a) An SEM image of 7 wt% BSMS-PiG, and EDS mapping of the elements contained in the BSMS phosphor and glass matrix. (b) A photograph of the 7 wt% BSMS-PiG sample under 365 nm UV light. (c) A surface fluorescence distribution image; and (d and e) 3D reconstruction images of the 7 wt% BSMS-PiG sample.

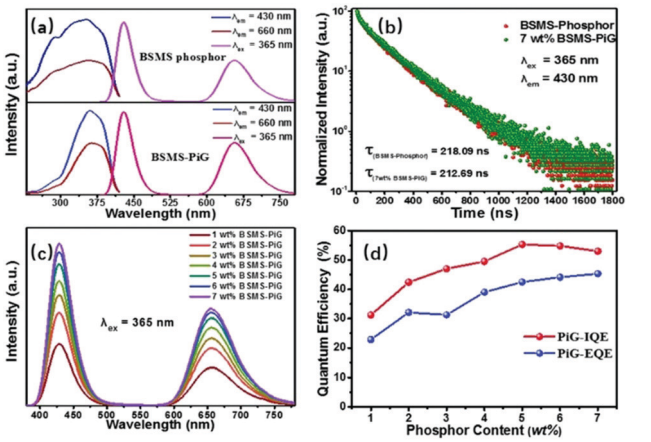

Fig. 2 (a) PLE spectra, PL spectra and (b) luminescence decay curves of the BSMS phosphor and 7 wt% BSMS-PiG. (c) PL spectra and (d) quantum efficiencies of BSMS-PiG with different phosphor doping concentrations.

measured under 365 nm excitation at 25 °C to further prove the potential of BSMS-PiG for practical application. As displayed in Fig. 2d, there is an overall upward trend in quantum efficiencies for the BSMS-PiG samples with increasing phosphor doping concentration; the maximum IQE value is obtained at 5 wt% BSMS-PiG and the maximum AE and EQE values present at 7 wt% BSMS-PiG. However, compared with the BSMS phosphor (EQE = 57.54%), the EQE of BSMS-PiG is dramatically lower. This phenomenon has been described in numerous previous articles[30–32] and this efficiency loss is acceptable to improve the chemical stability of the BSMS phosphor. Therefore, combining the above results, it can be seen that 7 wt% BSMS-PiG has great potential for high-power plant lighting.

It is widely acknowledged that the thermal stability of luminescence is a significant factor in assessing the application of luminescent materials in high-power LED devices. In this context, the temperature-dependent PL spectra of 7 wt% BSMS-PiG and the phosphor sample were measured. As shown in Fig. 3a and b, the Eu^{2+} emission bands (380–500 nm) manifest an apparent thermal quenching but the emission intensity of the Mn^{2+} emission bands (580–780 nm) increases as the temperature increases under 365 nm excitation. What needs to be mentioned here is the anti-Stokes effect.[33] Generally, the emission intensity of a fluorescence spectrum can be defined as follows:[34]

$$I \propto ANhv$$

where I is the emission spectrum intensity, A is the autonomous transition probability, N is the electron population, h is the Planck constant, and v is the emitting light frequency. The electron population in the vibrational ground state dwindles with increasing temperature. On the contrary, the electron populations in the vibrational excitation states rise up.

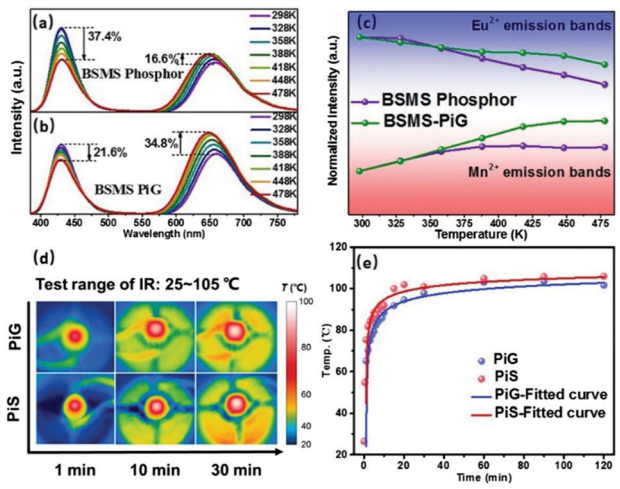

Fig. 3 Temperature-dependent PL spectra of (a) the BSMS phosphor and (b) 7 wt% BSMS-PiG recorded from 298 to 478 K. (c) The variation of the corresponding normalized PL intensities of the BSMS phosphor and 7 wt% BSMS-PiG. (d) Thermal images of BSMS-converted LED chips and BSMS-PiS-converted LED chips with 1 A current after different operating times, and (e) temperature as a function of the time of operation.

Accordingly, the emission intensity of anti-Stokes emission increases which partially compensates for the intrinsic temperature quenching effect of the material, as seen in the phenomenon of the Mn^{2+} emission bands (550–780 nm) with rising temperature. The thermal quenching of 7 wt% BSMS-PiG is less influenced by temperature than the BSMS phosphor. Furthermore, the intensity of the anti-Stokes emission bands in 7 wt% BSMS-PiG demonstrates much more temperature dependence than that in the BSMS-phosphor, because the anti-Stokes effect prevails over the thermal quenching effect. As shown in Fig. 3c, the normalized intensities of the BSMS phosphor and 7 wt% BSMS-PiG in the blue emission region are respectively reduced to 0.626 and 0.784 at 475 K, and the normalized intensities of the BSMS phosphor and 7 wt% BSMS-PiG in the red emission region are respectively increased by 16.6% and 34.8%, relative to the intensities at 298 K. For many plants, red light promotes the growth of the stem, leaf and fruit to a greater extent than blue light during the plant growth cycle. Therefore, the anti-Stokes effect of BSMS-PiG is suitable for application in high-power lamps for plant cultivation.

In addition, the thermal transfer phenomena were evaluated by thermographic images that revealed the concentric distribution of thermal energy on the surface of the BSMS-PiG and BSMS-PiS, as shown in Fig. 3d. BSMS-PiG shows a broader radial temperature gradient zone than BSMS-PiS. The increase in the area over which the thermal energy has spread means that the convection process is more effective. The temperatures as a function of time are plotted in Fig. 3e. The surface temperatures experienced a dramatic rise when the LED chips were turned on, and then reached a maximum of 100 °C after 30 min. The BSMS-PiG showed temperatures that were 3.1–11.2% lower at the surface compared with the temperatures of BSMS-PiS. This phenomenon is because the BSMS-PiG has a higher thermal conductivity ($\sim$1.242 W m^{-1} K^{-1}) than that of BSMS-PiS ($\sim$0.16 W m^{-1} K^{-1}) and contributes to the spreading of the heat. This can weaken the thermal quenching of the embedded BSMS phosphor.

The energy required for plant growth and morphogenesis is mainly provided by light energy, especially from blue, red, and far red light. The emission spectrum of BSMS-PiG exactly matches the absorption of plant pigments. Therefore, BSMS-PiG was used to assemble plant lights as shown in Fig. 4a and b. However, the wavelengths of light required for the growth of different plants can differ,[35] thus it is of great significance to be able to regulate the ratio of blue light to red light for the growth of different plants. Here, the PL spectra of different thicknesses of 7 wt% BSMS-PiG and different concentrations of Mn^{2+} ions in the BSMS-PiG-converted $\sim$370 nm LED chips were determined, and these spectra showed different red-blue ratios, as exhibited in Fig. 4c and d. The proportion of blue light decreases, the proportion of red light increases and the overall luminescence intensity decreases as the thickness of BSMS-PiG increases. As the propagation path of the light in the glass gets longer, blue light is absorbed by phosphor to excite red light, thus changing the ratio of blue to red. In addition, the effect of changing thickness on absorptivity (abs.) and conversion

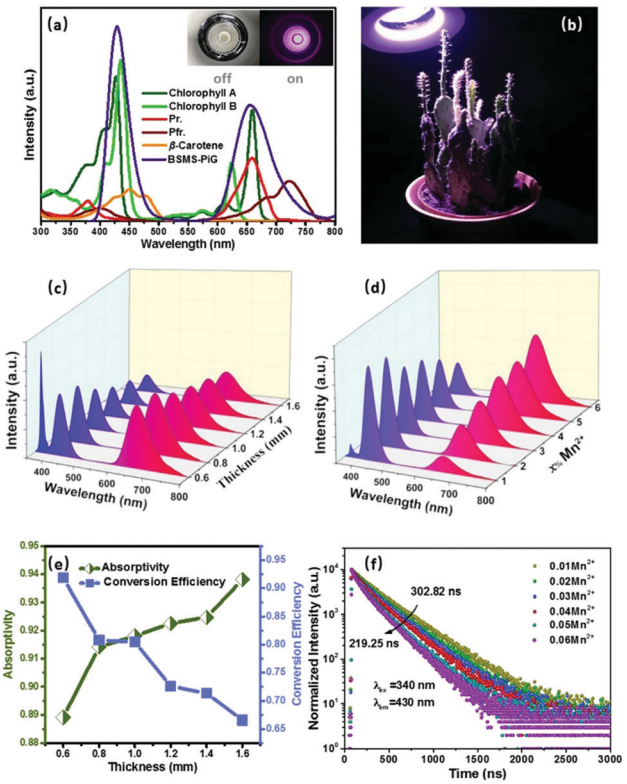

Fig. 4 (a) Plant photosynthesis absorption spectrum, and PL spectrum of the 7 wt% BSMS-PiG-converted ~370 nm LED chips. (b) A schematic diagram of the plant lamp concept. Spectra of different BSMS-PiG plant lamps with different blue-red ratios with (c) 7 wt% BSMS-PiG at various thicknesses, and (d) different concentrations of Mn^{2+} doping in the BSMS phosphors at a BSMS-PiG thickness of 1.0 mm. (e) The effect of changing thickness on the absorptivity and conversion efficiency of 7 wt% BSMS-PiG. (f) The luminescence decay curves of 7 wt% BSMS-PiG at 430 nm.

efficiency (η_c) of 7 wt% BSMS-PiG is exhibited in Fig. 4e, and calculated according to the following equations:

$$\text{abs.} = \frac{\int[\text{Ex}(\lambda) - T(\lambda)]\text{d}\lambda}{\int \text{Ex}(\lambda)\text{d}\lambda}$$

$$\eta_c = \frac{\int \text{Em}(\lambda)\text{d}\lambda}{\int[\text{Ex}(\lambda) - T(\lambda)]\text{d}\lambda}$$

where $\text{Ex}(\lambda)$, $\text{Em}(\lambda)$ and $T(\lambda)$ are the intensities per unit wavelength in the excitation, emission and transmitted light spectra of BSMS-PiG, respectively. The absorption of UV light by the glass substrate increases because of the increasing thickness of BSMS-PiG so the phosphors in the glass cannot be completely excited, and there is a downward trend in overall luminescence intensity. It is well understood that the red-blue ratio can be adjusted by reasonably increasing the concentration of phosphor doped Mn^{2+} ions in the same conditions. The luminescence lifetime of Eu^{2+} ion decreases gradually (Fig. 4f) when the concentration of Mn^{2+} increases from 1 to 6 mol%. This is mainly due to the increasing luminescence of Mn^{2+} ions and the energy transfer between Eu^{2+} and Mn^{2+}.[36] (The specific efficiency of energy transfer is given in the ESI,† Fig. S5.) As the

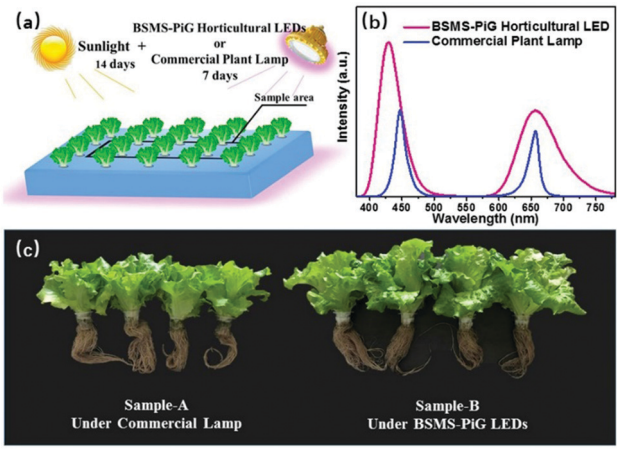

Fig. 5 (a) A schematic diagram showing Romaine lettuce cultivation with irradiation from different light sources. (b) PL spectra of the BSMS-PiG horticultural LED and the commercial plant lamp. (c) A photograph of Romaine lettuce cultivated under different light treatments.

concentration of Mn^{2+} increases from 1 to 6 mol%, the PL intensity of Eu^{2+} decreases monotonically, whereas the PL intensity of Mn^{2+} increases. The PL intensity ratio of blue to red changes from around 1 : 0.3 to 1 : 3.5.

Finally, the influence of light treatment on Romaine lettuce growth was tested using the 7 wt% BSMS-PiG plant lamp, and a reference commercial plant lamp (Fig. 5a). The middle part of the planting area was used as a reasonable sample selection area to ensure the evenness of illumination and the reliability of the experiment. The PL spectra of the two kinds of horticultural LEDs are given in Fig. 5b, and demonstrate that the BSMS-PiG plant lamp has almost the same emission peaks as the commercial plant growth LEDs, but the full width at half-maxima of the former (~44 nm in the blue region, 79 nm in the red region) are obviously wider than those of the latter (~25 nm in the blue region, 24 nm in the red region). The benefit of cultivating the Romaine lettuces under the BSMS-PiG plant lamp is clear. After cultivation for 3 weeks, the Romaine lettuces receiving light treatment from the BSMS-PiG-converted ~370 nm LED chips have greener and bigger leaves than those cultivated with the commercial plant lamp, as presented in Fig. 5c; the comparison between lettuces from the sample groups A and B can be clearly seen. In addition, for further detailed verification, parameters relating to the biomass of the plants are listed in Table 1. These include quality index, chlorophyll content, β-carotene content and soluble protein content. Samples from group A (cultivated under irradiation from the BSMS-PiG horticultural LEDs) have better physiological measures than samples from group B (cultivated under irradiation from the commercial plant lamp): fresh weight is increased by 62.58%, dry weight is increased by 58.27%, total chlorophyll content is 26.05% higher, β-carotene content is 22.82% higher and soluble protein content is 21.40% higher. The results of this experiment on the indoor cultivation of Romaine lettuces indicate that the BSMS-PiG horticultural LEDs offer a superior light source for facilitating plant growth, increasing crop yield,

Table 1 Effects of different light sources on the indicators of Romaine lettuce samples

	Fresh weight (g plant^{-1})	Dry weight (g plant^{-1})	Total chlorophyll content (mg g^{-1})	β-Carotene content (mg g^{-1})	Soluble protein content (mg g^{-1})
A	26.224 ± 4.7	1.215 ± 0.18	0.787 ± 0.03	0.149 ± 6‰	2.051 ± 0.25
B	42.636 ± 4.8	1.923 ± 0.29	0.992 ± 0.02	0.183 ± 2‰	2.490 ± 0.15

accelerating product morphology and boosting nutrient content. Consequently, the BSMS-PiG horticultural LEDs with their brilliant spectral characteristics are a potential candidate for a high-power horticultural light source to replace conventional plant lamps.

4 Conclusions

In summary, $Ba_{1.3}Sr_{1.7}MgSi_2O_8:Eu^{2+},Mn^{2+}$ (BSMS) phosphors with bright dual-broadband emission were synthesized by a conventional high-temperature solid-state method, and the phosphors were further developed as stable light convertors through a phosphor-in-glass (PiG) approach for high-power horticultural LEDs. BSMS-PiG retains the luminescence properties of the BSMS phosphor and gives a high external quantum efficiency of 45.3%. Compared to the BSMS phosphor, BSMS-PiG exhibits better thermal stability in the temperature range of 298 to 478 K. Not only that, but BSMS-PiG shows superior thermal conductivity ($\sim$1.242 W m^{-1} K^{-1}), which contributes to heat spreading to reduce the thermal quenching of the embedded BSMS phosphor. Furthermore, the blue-red intensity ratio of a BSMS-PiG plant lamp could be adapted to optimise the growth of different plants by controlling the thickness of the BSMS-PiG and the concentration of doped Mn^{2+} ions in BSMS-PiG-converted $\sim$370 nm LED chips. The results of an experiment on the indoor cultivation of Romaine lettuce indicate that BSMS-PiG, with its brilliant spectral characteristics and superior thermal stability, is an ideal candidate light convertor for high-power horticultural LEDs.

Conflicts of interest

There are no conflicts to declare.

Acknowledgements

The present work was supported by the National Natural Science Foundations of China (Grant No. 21671070); the Project of GDUPS (2018) for Prof. Bingfu LEI; the Guangzhou Science & Technology Project, China (No. 201704030086); and the National Undergraduate Innovation and Entrepreneurship Training Program grant for Gening Xie (No. 201910564035).

Notes and references

1 J. Zhan, I. Twardowska, S. Wang, S. Wei, Y. Chen and M. Ljupco, *J. Cleaner Prod.*, 2019, **212**, 22–36.
2 J. D. B. Gil, P. Reidsma, K. Giller, L. Todman, A. Whitmore and M. van Ittersum, *Ambio*, 2019, **48**, 685–698.
3 C. A. Mitchell, in *VII International Symposium on Light in Horticultural Systems*, ed. S. Hemming and E. Heuvelink, 2012, vol. 956, pp. 23–36.
4 X. Pan, D. Li, Y. Fang, Z. Liang, H. Zhang, J. Z. Zhang, B. Lei and S. Song, *J. Phys. Chem. Lett.*, 2020, DOI: 10.1021/acs.jpclett.9b03740.
5 M. Xia, X. Wu, Y. Zhong, Z. Zhou and W.-Y. Wong, *J. Mater. Chem. C*, 2019, **7**, 2385–2393.
6 R. Dong, Y. Li, W. Li, H. Zhang, Y. Liu, L. Ma, X. Wang and B. Lei, *J. Rare Earths*, 2019, **37**, 903–915.
7 C. M. Bourget, *HortScience*, 2008, **43**, 1944–1946.
8 Z. Xia and Q. Liu, *Prog. Mater. Sci.*, 2016, **84**, 59–117.
9 X. Yang, Y. Zhang, X. Zhang, J. Chen, H. Huang, D. Wang, X. Chai, G. Xiue, M. S. Molokeev, H. Zhang, Y. Liu and B. Lei, *J. Am. Ceram. Soc.*, 2020, **103**, 1773–1781.
10 E. Darko, P. Heydarizadeh, B. Schoefs and M. R. Sabzalian, *Philos. Trans. R. Soc., B*, 2014, **369**, 20130243.
11 M. H. Chang, D. Das, P. V. Varde and M. Pecht, *Microelectron. Reliab.*, 2012, **52**, 762–782.
12 R. Zhang, H. Lin, Y. Yu, D. Chen, J. Xu and Y. Wang, *Laser Photonics Rev.*, 2014, **8**, 158–164.
13 S. Nishiura, S. Tanabe, K. Fujioka and Y. Fujimoto, *Opt. Mater.*, 2011, **33**, 688–691.
14 N. Wei, T. Lu, F. Li, W. Zhang, B. Ma, Z. Lu and J. Qi, *Appl. Phys. Lett.*, 2012, **101**, 061902.
15 D. Chen, Y. Zhou, W. Xu, J. Zhong, Z. Ji and W. Xiang, *J. Mater. Chem. C*, 2016, **4**, 1704–1712.
16 B. Wang, H. Lin, F. Huang, J. Xu, H. Chen, Z. Lin and Y. Wang, *Chem. Mater.*, 2016, **28**, 3515–3524.
17 J. Deng, H. Zhang, X. Zhang, Y. Zheng, J. Yuan, H. Liu, Y. Liu, B. Lei and J. Qiu, *J. Mater. Chem. C*, 2018, **6**, 1738–1745.
18 M. Li, X. Zhang, H. Zhang, W. Chen, L. Ma, X. Wang, Y. Liu and B. Lei, *J. Mater. Chem. C*, 2019, **7**, 3617–3622.
19 S. M. Zahedi and H. Sarikhani, *Russ. J. Plant Physiol.*, 2017, **64**, 83–90.
20 S. Oh and B. L. Montgomery, *Cell*, 2017, **171**, 1254–1256.
21 E. Kim, S. Unithrattil, I. S. Sohn, S. J. Kim, W. J. Chung and W. B. Im, *Opt. Mater. Express*, 2016, **6**, 255933.
22 J. He, L. Qin, E. L. Chong, T. W. Choong and S. K. Lee, *Front. Plant Sci.*, 2017, **8**, 361.
23 L. Cao, Q. Lu, L. Wang, J. Li, J. Song and D. Wang, *Ceram. Int.*, 2013, **39**, 7717–7720.
24 J. K. Han, A. Piqutte, M. E. Hannah, G. A. Hirata, J. B. Talbot, K. C. Mishra and J. McKittrick, *J. Lumin.*, 2014, **148**, 1–5.
25 L. Sun, Q. Lu, Z. Mao and D. Wang, *J. Mater. Sci.: Mater. Electron.*, 2015, **26**, 2647–2653.

26 Z. Mao, J. Chen, L. Sun, Q. Lu and D. Wang, *Mater. Res. Bull.*, 2015, **70**, 908–913.
27 J. Zhang, L. Dong and S.-H. Yu, *Sci. Bull.*, 2015, **60**, 785–791.
28 Y. Zheng, G. Xie, X. Zhang, Z. Chen, Y. Cai, W. Yu, H. Liu, J. Shan, R. Li, Y. Liu and B. Lei, *ACS Omega*, 2017, **2**, 3958–3965.
29 Z. Tian, Y. Qiu and J. Cai, *Ceram. Int.*, 2016, **42**, 6369–6374.
30 H. Segawa, S. Ogata, N. Hirosaki, S. Inoue, T. Shimizu, M. Tansho, S. Ohki and K. Deguchi, *Opt. Mater.*, 2010, **33**, 170–175.
31 H. Lin, T. Hu, Y. Cheng, M. Chen and Y. Wang, *Laser Photonics Rev.*, 2018, **12**, 1700344.
32 M. Li, H. Zhang, X. Zhang, J. Deng, Y. Liu, Z. Xia and B. Lei, *Mater. Res. Bull.*, 2018, **108**, 226–233.
33 J. Chen, W. Zhao, N. Wang, Y. Meng, S. Yi, J. He and X. Zhang, *J. Mater. Sci.*, 2016, **51**, 4201–4212.
34 R. N. Zare, *J. Chem. Phys.*, 1964, **40**, 1934–1944.
35 S. Dutta Gupta and B. Jatothu, *Plant Biotechnol. Rep.*, 2013, **7**, 211–220.
36 Y. Sun, P. Li, Z. Wang, J. Cheng, Z. Li, C. Wang, M. Tian and Z. Yang, *J. Phys. Chem. C*, 2016, **120**, 20254–20266.

